Induced Orientational Order in Symmetric Diblock Copolymer Thin Films**

By *Ricardo Ruiz*,* *Robert L. Sandstrom*,* and *Charles T. Black*

Block-copolymer self-assembly has proven to be an attractive fabrication method for nanotechnology applications because of its ability to precisely define regular patterns with dimensions in the range of 10 to 100 nm.[1,2] Thin films of cylindrical and spherical patterns have been successfully used as lithographic templates in electronics applications[3–8] that require an optimal mask profile along with a minimum number of defects. Thin films of lamellar diblock copolymers have an advantageous profile for lithographic applications involving striped patterns;[2,9,10] however, their coarsening dynamics (i.e., pattern-forming properties) have not been as fully characterized as those of their asymmetric counterparts,[11–13] and their utility is not yet demonstrated.

In this Communication we present a new polymer multilayer fabrication method — analogous to heteroepitaxial film growth — employing thin films of lamellar polystyrene-*block*-poly(methyl methacrylate) (PS-*b*-PMMA). We also demonstrate the effectiveness of the technique by patterning silicon wire arrays with a 20 nm width and a 35 nm center-to-center spacing. In understanding the pattern-formation properties of lamellar-phase PS-*b*-PMMA, we find that orientational correlations in symmetric (lamellar) thin films evolve much more slowly with time than in asymmetric (cylindrical) films, limiting their use in applications that require long-range orientational order. To overcome this limitation, we demonstrate a multilayer pattern-formation process that features defect-free lamellar pattern formation.

Diblock copolymer thin films of cylindrical and lamellar phases both form striped patterns that coarsen with annealing time (t) according to the power law $\xi(t) \sim t^\phi$,[14,15] where ξ is a correlation length associated with grain size, and ϕ is termed the growth exponent. Striped patterns form from parallel oriented cylindrical-phase films and perpendicular lamellar domain orientations. Considerable previous theoretical work has described both the formation and evolution of generalized striped patterns[16–18] as well as two-dimensional lamellar block copolymers,[19–23] with predictions for ϕ ranging from 0.2 to 0.5. Experimentally, Harrison et al. first measured the time evolution of $\xi(t)$ in cylindrical phase PS-*b*-PI diblock copolymer thin-films,[24] finding a value for ϕ of 0.25. Earlier experimental work by Garetz et al.[25] measured ξ in bulk lamellar diblock copolymers. From their data, one can estimate a value for ϕ in the range of 0.066–0.131, i.e., significantly lower than $\phi = 0.25$. Despite their relevance in lithographic applications, correlations on thin films of symmetric diblock copolymers have been studied less.

We prepared thin-film striped patterns of both parallel PS-*b*-PMMA cylinders (Fig. 1a) and perpendicular PS-*b*-PMMA lamellae (Fig. 1b and c) to compare the time evolution of ξ. We spin-casted thin films of cylindrical and lamellar materials, and annealed them (195 °C in vacuum) for times ranging from 5 to 4000 minutes. Cylindrical-phase PS-*b*-PMMA films were cast at a thickness suitable to form a single layer of parallel cylindrical domains (25 nm). Perpendicular lamellar materials form striped patterns for film thicknesses close to either the natural lamellar period, L_o (32 nm, in our films), or $(1/2)L_o$.[26] We ensured perpendicular orientation of the lamellar domains by surface pretreatment with a random copolymer brush[27] prior to diblock copolymer application.

The orientational correlation length (ξ) of our parallel cylindrical PS-*b*-PMMA films (solid circles, Fig. 1d) increases much more rapidly with time than the ξ of our perpendicular PS-*b*-PMMA lamellar films (open squares and solid triangles). We measured a kinetic exponent $\phi = (0.26 \pm 0.01)$ for cylindrical films, which is consistent with $\phi = 0.25$ that was previously reported for cylindrical-phase poly(styrene)-*block*-poly(isoprene) (PS-*b*-PI) diblock copolymers.[24] For lamellar films of thicknesses approximately equal to L_o (open squares), ξ remained nearly constant for all annealing times (indicating a constant defect density). We note that samples annealed for short times (< 10 min) were subject to a greater experimental uncertainty because of temperature fluctuations during the sample loading and unloading processes, so we cannot at present comment on the time-dependence of ξ for short anneal times. Striped patterns of films with a thickness of $(1/2)L_o$ (solid triangles) coarsen slightly with time, with $\phi = 0.11 \pm 0.01$.

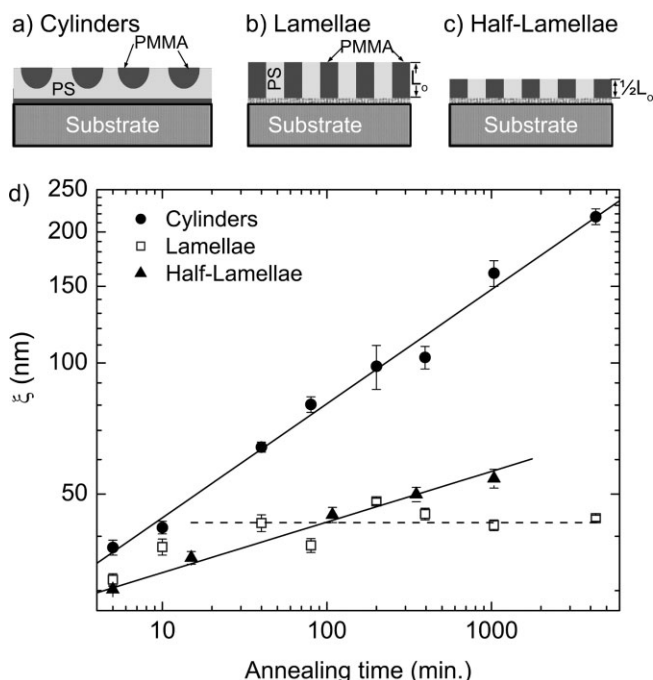Here, we briefly assess probable causes for a reduced rate of striped-pattern coarsening of PS-*b*-PMMA lamellae rela-

[*] Dr. R. Ruiz,[+] R. L. Sandstrom, Dr. C. T. Black[++]
IBM T. J. Watson Research Center
Yorktown Heights, NY 10598 (USA)
E-mail: ricardo.ruiz@hitachigst.com; rlsands@us.ibm.com

[+] Present address: Hitachi Global Storage Technologies, 3403 Yerba Buena Rd., San Jose, CA 95135, USA.

[++] Present address: Brookhaven National Laboratory, Center for Functional Nanomaterials, Building 555, Upton, NY 11973, USA.

a) Cylinders b) Lamellae c) Half-Lamellae

Figure 1. a–c) Cross-sectional schematics of diblock copolymer thin films. a) Parallel cylinders. b) Perpendicular lamellae of thickness L_o. c) Perpendicular lamellae of thickness $(1/2)L_o$. d) Measurements of the correlation length, ξ, versus annealing time for PS-*b*-PMMA thin films of parallel cylinders (●), perpendicular lamellae (□), and perpendicular half-lamellae (▲).

tive to PS-*b*-PMMA cylinders. One apparent difference between the two systems is that the parallel cylinder striped pattern forms on a PS-*b*-PMMA brush layer (with PMMA wetting the SiO surface),[28] while the perpendicular lamellar striped pattern forms on a polystyrene-*random*-poly(methyl methacrylate) (PS-*r*-PMMA) copolymer brush.[27] Previous kinetic studies of perpendicular PS-b-PMMA cylinder patterns on similar PS-*r*-PMMA copolymer brushes[29] measured ϕ values of ca. 0.25, indicating that coarsening is not inhibited by the random copolymer.

Available data also suggests similar polymer diffusion rates in PS:PMMA cylinders and lamellae. Polymer diffusion along microdomains (i.e., parallel to pattern stripes) is favored over diffusion across domains, because of the enthalpic penalty associated with block mixing.[30–35] For nonentangled block copolymers, the parallel (D_{par}) and perpendicular (D_{perp}) diffusion constants are given by[30,33]

$$D_{par} \approx D_o$$

$$D_{perp} \sim D_o\, e^{-a\xi N_A} \qquad (1)$$

where $D_0 = \dfrac{k_B T}{N\zeta}$ is the Rouse-model diffusion constant,[36] a is a parameter of order 1,[30,37] N_A is the degree of polymerization of the core block (cylinders) or the longest block (la-

mellar),[30] and ζ is the monomeric friction factor. In our materials, D_o is limited by the PMMA block ($\zeta_{PMMA}/\zeta_{PS} \approx 10^3$), and thus we estimate $D_o \approx 10^{-12}$ cm^2 s^{-1} for both cylinders and lamellae[38] (both have a similar PMMA content, see Experimental). While there is no available data for either a or the proportionality constants for our exact materials, measurements of similar systems[33,34] indicate that we can expect a largely restricted D_{perp} value in both cases.
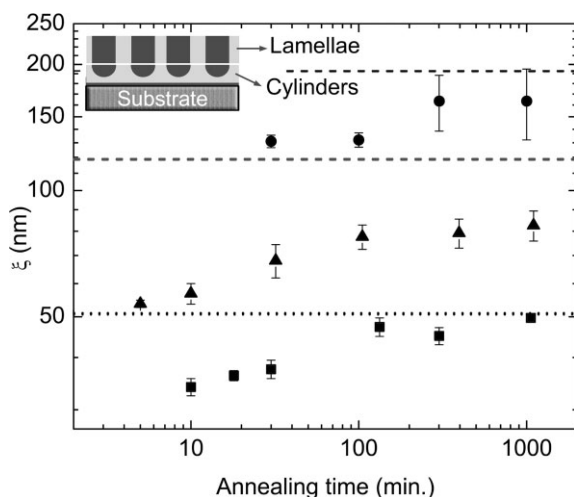
The pattern coarsening of PS-*b*-PMMA lamellar striped patterns is also not limited by polymer entanglement, as we estimate this effect to be more pronounced in our cylindrical material (which nonetheless coarsens faster than the lamellar pattern). Chain entanglement occurs above a critical molecular weight M_c, which is ca. 31.2–38 kg mol^{-1} for PS[38] and 27.5–31.5 kg mol^{-1} for PMMA.[38] In our experiments, the only block with a number-average molecular weight (M_n) larger then M_c is the PS block in the PS:PMMA cylindrical material ($M_n = 42.2$ kg mol^{-1}); all other blocks are nonentangled, with $M_n < M_c$.

Our measurements suggest that topological differences between cylindrical and lamellar morphologies influence coarsening kinetics. At present, there is no model that connects the diffusion of individual molecules to defect motion and annihilation, so we discuss the effect of film morphology in general terms. In smectic phases, defect motion by climb (dislocation displacement parallel to layer planes) is favored over glide (dislocation displacement perpendicular to the layers) because glide requires layer breaking;[39] however, defect-annihilation processes necessarily involve glide. Differences in the required energy for layer breaking (i.e., glide) may play a role in the observed difference in domain coarsening. We understand the origin for such an energy difference by noting that in the cylindrical striped pattern it is possible to glide without traversing a cylindrical domain, as molecules can diffuse or rotate around cylinder cores[23] (with the favorable D_{par}). In lamellar striped patterns, glide necessarily involves molecular diffusion across domains with the slower D_{perp}.

Different film-stress energy values in lamellar and cylindrical materials during defect annihilation may also contribute to the differences in pattern-coarsening kinetics. Disclination defects of opposite sign attract each other,[40] and this attraction drives defect motion and ultimately annihilation in cylindrical phase films.[11,24,41,42] In 2D lamellar films this attractive force is balanced by the repulsive force of layer compression, which prevents defects of opposite sign from approaching a distance less than a critical number of periods (n_c).[40] The magnitude of these attractive and repulsive forces may differ considerably between lamellar and cylindrical morphologies because of the differences in the density profiles. At present, we cannot uniquely identify the mechanism for the observed difference in coarsening kinetics, however this discussion identifies likely candidates originating from topological materials differences for future investigation.

The extremely slow rate at which PS-*b*-PMMA lamellar-phase striped patterns coarsen with annealing time complicates their use in applications that require large defect-free

pattern areas. Chemical nanopatterning[43] has previously been demonstrated to direct defect-free assembly of lamellar phase materials over large areas[44] and onto nonregular patterns,[45] and here we extend this concept to a multilayer approach, where a first, parallel-oriented, cylindrical-phase layer templates the ordering of a second, perpendicularly oriented, layer of lamellar-phase material (inset in Fig. 2).
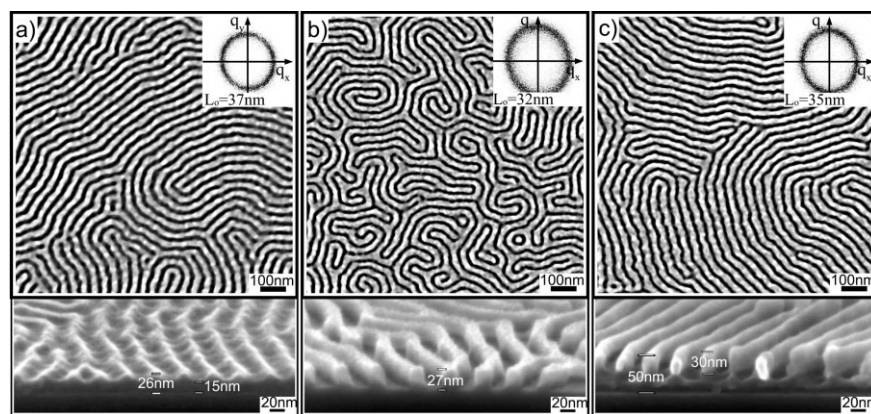

Figure 2. Time evolution of the correlation length of lamellar films deposited on top of three different underlayer cylindrical templates. (■), (▲), and (●) correspond to films deposited on templates with $\xi_{cyl} = (51 \pm 2)$ nm, $\xi_{cyl} = (119 \pm 15)$ nm, and $\xi_{cyl} = (193 \pm 33)$ nm, respectively (ξ_{cyl} values shown as dashed lines). Inset: schematic representation of the stacked layer configuration.

In a double-layer structure, the cylinder underlayer acts as a template for the top lamellar film layer. We produced three different cylinder underlayer templates, having three different correlation lengths: $\xi_{cyl} = (51 \pm 2)$ nm, (119 ± 15) nm, and (193 ± 33) nm (dashed lines in Fig. 2). The underlayer template patterns were immobilized and rendered insoluble by crosslinking the polystyrene with UV-light. Subsequently, we deposited lamellar top-layer films on each of the three underlayer templates. In all three cases (squares, triangles, and circles in Fig. 2), the correlation length of the lamellar film (ξ_{lam}), coarsens with annealing time and asymptotically approaches that of the respective underlayer film, indicating an induced ordering by the template underlayer. The correlation length of the lamellar film reached its saturated value after 100 min of annealing. Although saturated values of ξ_{lam} are lower than ξ_{cyl} of their associated cylinder under-

layers, the multilayer approach provides a method for enhancing ξ_{lam} from ca. 45 nm in a single lamellar layer (with no underlayer) to ca. 160 nm in a double-layer configuration (with template $\xi_{cyl} = 193$ nm).

Visual inspection of scanning electron microscopy (SEM) images confirms the induced order imposed on the top layer lamellar film by the cylinder underlayer template (Fig. 3). Figure 3a shows a typical cylinder underlayer with $\xi_{cyl} = 217$ nm and a thickness of ca. 25 nm). PMMA is removed to improve image contrast by exposure to UV-radiation and immersion in acetic acid.[10,46] A perpendicular-oriented lamellar striped pattern (Fig. 3b) with a thickness of ca. 27 nm has $\xi_{lam} \approx 45$ nm, regardless of annealing time. The lamellar phase correlation length is enhanced in the double-layer configuration (Fig. 3c) of a lamellar top layer deposited on top of a cylinder underlayer template. The correlation lengths of the lamellar top layer film and its underlayer template are $\xi_{lam} = 164$ nm and $\xi_{cyl} = 193$ nm, respectively. The cross section of the film (Fig. 3c) shows a dark scalloped film on the substrate, which we associate with the original cylinder underlayer (ca. 20 nm thick), and a lamellar top layer of a lighter color. Cross-sectional images reveal the main differences between these materials for lithographic applications. In cylindrical films, the substrate is not neatly exposed at the bottom of the cylinder cavity (ca. 15 nm of polymer remains), while lamellar patterns are clear from top to bottom and provide an efficient mask for processes such as plasma etching. The double-layer process also improves the aspect ratio of the film for lithographic applications, even though this film still contains an underlayer of ca. 20 nm.

Figure 3. a–c) Representative SEM images of the three different types of films. a) Thin film of a cylindrical phase with $\xi_{cyl} = 217$ nm. The bottom image shows a cross-sectional SEM image (X-SEM) revealing an approximate film thickness of ca. 26 nm. The inset shows the power spectral density (PSD) from which a repeat unit, L_o, was extracted. b) Thin film of a lamellar phase with $\xi_{cyl} = 45$ nm. The short correlation length is evident when compared to (a). The cross-sectional image below, however, shows that after PMMA removal, the pattern is cleared down to the substrate, providing an efficient mask for lithographic processes. c) Enhancement of the correlation length of the lamellar phase deposited on top of a cylindrical thin film in a double-layer configuration. The correlation lengths of the lamellar and of the underlayer cylindrical films are $\xi_{lam} = 164$ nm and $\xi_{cyl} = 193$ nm, respectively. The cross-sectional SEM image at the bottom reveals a dark thin film above the substrate that we associate with the original cylindrical template followed by the lighter-colored lamellar second layer.

The lamellar top layer period, L_o, is modified by the period of the cylinder underlayer template. Thin films of the cylindrical phase, lamellar phase, and lamellar-on-cylinder underlayer template have average periods of $L_{cyl} = 37$ nm, $L_{lam} = 32$ nm and $L_{dbl} = 35$ nm, respectively, measured from the first order peak in the power spectral density, which is the magnitude squared of the Fourier transform (insets in Fig. 3). The smaller natural lamellar period (32 nm) is stretched in accommodating the lattice difference while reproducing the pattern underneath (period 37 nm), although in the end there still exists a lattice mismatch of $1 - L_{dbl}/L_{cyl} = (1 - 35$ nm$/37$ nm$) = 0.05$, or 5%. This mismatch may partially explain why the correlation length of the double-layer film never reaches that of the cylinder underlayer template. Improved induced order may be possible by choosing cylindrical and lamellar materials with identical intrinsic periods or by adjusting polymer periods through homopolymer blending.[45]

We use the multilayer induced ordering approach not only to improve the coarsening kinetics of lamellar films, but also to align lamellar films to pre-existing lithographic patterns. Conventional lithography and etching creates patterned trenches 270 nm wide by 20 nm deep, which then template the assembly of a cylindrical-phase PS-b-PMMA film (Fig. 4a) such that after annealing the cylinder domains span the trench width and run free of defects over several micrometers.[47–49] A similar trench with the bottom surface treated with a PS-r-PMMA copolymer brush[27] results in an unaligned lamellar striped pattern (Fig. 4b) that contains a high density of defects. Applying a lamellar film on top of an oriented cylindrical underlayer (shown in Fig. 4a) results in an aligned lamellar pattern in registration with the cylinder template below (Fig. 4c). Outside of the lithographic trench (where there is no cylinder template), the lamellar striped pattern remains unaligned and uncoarsened. We have used aligned double-layer structures as lithographic masks for the fabrication of silicon wire arrays with nanometer-scale dimensions (width 15 nm, pitch 32 nm, and height 36 nm, Fig. 4d). In this example we etched Si by using SF_6 gas chemistry and removed remaining polymer with an O_2 plasma.

We have demonstrated a new fabrication method by using aligned perpendicular-oriented lamellar materials as lithographic templates. We have also found that the correlation length in cylindrical polystyrene-block-poly(methyl methacrylate) (PS-b-PMMA) films follows the same scaling law as previously measured for cylindrical phase PS-b-PI,[24] while PS-b-PMMA lamellar films evolve much more slowly with time, limiting their applicability where long-range orientational order is needed. Our successful implementation required a multilayer configuration employing a cylindrical thin-film template to induce ordering in an overlaying lamellar film.
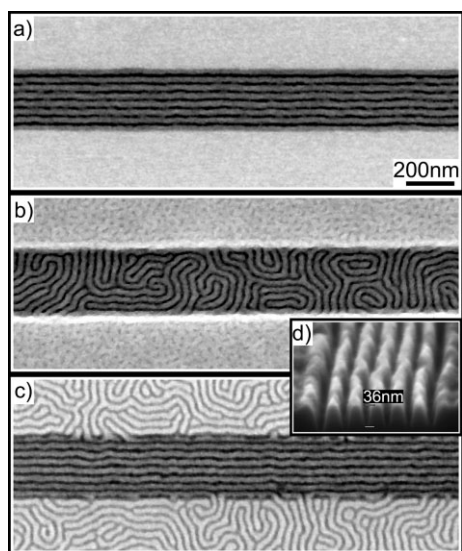
Experimental

PS-b-PMMA with a total number-average molecular weight of 64 kg mol^{-1}, a weight ratio 70:30 (PS:PMMA), and a polydispersity index (PDI, defined as the quotient of the weight- and number-average molecular weights (M_w/M_n) of 1.16 was used to form PMMA cylinders in a PS matrix. This polymer was synthesized at IBM Almaden Research Center by controlled living free-radical polymerization, resulting in highly atactic content. Lamellae-forming PS-b-PMMA was purchased from Polymer Source Inc., with $M_n = 51$ kg mol^{-1}, weight ratio 50:50 (PS:PMMA) and $M_w/M_n = 1.09$, and was synthesized by living anionic polymerization with PMMA rich in syndiotactic content (>78%).

Prior to spin casting, Si substrates (with native silicon oxide) were sonicated for 5 min in acetone, rinsed with methanol, and blown dry with clean nitrogen. Thin films of the cylindrical phase were spin cast at 2500 rpm from a 1 wt% solution in toluene. Lamellar-phase thin-films were deposited at two different thicknesses: ca. 30 and 15 nm [26]. We ensured perpendicular lamellar domain orientation by surface pretreatment with a random copolymer brush [27] prior to diblock copolymer application. At the polymer/air interface, the difference in surface tension between PS and PMMA is small, resulting in a configuration with both domains exposed to the top surface [28,41] as depicted in Figure 1a–c. Samples were baked at 195 °C in vacuum for various times. The pattern formed uniformly across the entire sample (ca. 2 cm × 2 cm).

For the double-layer experiments, thin-films of the cylindrical phase, prepared as outlined above, were irradiated with UV light for 5 min (peak wavelength 254 nm, 18 mW cm^{-2}). UV radiation cross-links PS making it insoluble and scissions PMMA [10,46]. The samples were rinsed with toluene and a lamellar layer was spin cast on top of the cross-linked bottom layer and baked at 195 °C in vacuum for various times. We believe the cross-linked PS along with the leftover PMMA chains induce ordering in the second layer in a similar way as chemically nanopatterned [44] substrates do.

The computational analysis of the correlation length was similar to that described by Harrison and co-workers [11] and Yokojima and Shiwa [22]. The method computationally evaluated, at each point of an image, the local orientational parameter, $\psi(\vec{r}) = \exp[2i\theta(\vec{r})]$, where $\vec{r}$ is the position vector and θ is the orientation of the director [40], $\hat{n}(\vec{r})$, normal to the stripe pattern at position $\vec{r}$. To avoid size effects, the size and resolution of the images were such that the lateral dimension of the image was at least 15 times the correlation length and a full

Figure 4. a–c) Pattern registration on lithographically prepatterned substrates. a) Thin-film of a cylindrical phase in a silicon oxide lithographic trench. The striped pattern aligns free of defects along the trench walls. b) Lamellar phase thin film in the same type of trench. The pattern does not align regardless of annealing conditions. c) Lamellar phase thin film on top of a cylindrical film similar to the one shown in (a). d) Etched Si using the film in (c) as a lithographic mask.

period of the striped pattern at least 15 pixels wide. The direction of $\hat{n}(\vec{r})$ was obtained from a local gradient intensity $\hat{n}(\vec{r}) = \frac{\vec{\nabla} I}{|\vec{\nabla} I|}$ evaluated at $\vec{r}$. The intensity is given by the gray level of the pixel at $\vec{r}$. Numerically, the gradient was evaluated over a box of size $\sim L_o \times L_o$ centered at $\vec{r}$. θ is given by $\arctan[n_y/n_x]$. We then followed Harrison's procedure [50] and defined a sine and a cosine field: $|\vec{\nabla} I|^2 \sin(2\theta)$, $|\vec{\nabla} I|^2 \cos(2\theta)$. Each of these fields was smoothed out by Gaussian-averaging each point with its neighbors to produce a well-defined director at all points. A "smooth" matrix of the double angle was obtained: $2\theta = \arctan[|\vec{\nabla} I|^2 \sin(2\theta)/|\vec{\nabla} I|^2 \cos(2\theta)]$. The order parameter follows: $\psi(\vec{r}) = \exp[2i\theta(\vec{r})]$. The azimuthally averaged pair correlation function was then given by $g(\mathrm{r}) = \langle \psi(\vec{0})\psi^*(\vec{r})\rangle_c$. For randomly oriented grains, $g(\mathrm{r})$ exhibited an exponential decay of the form $g(\mathrm{r}) = \exp[r/\xi]$ and ξ can be extracted from an exponential fit to $g(\mathrm{r})$.

To extract the correlation length for a given sample, we applied the above method to at least four independent SEM images. The reported values correspond to the average value while the error bars represent the standard deviation.

To measure the periodicity of the striped patterns, we performed a standard fast Fourier transform to a square SEM image. The power spectral density (PSD) was then circularly averaged, and the value of L_o was extracted from the position of the first order peak, k_o ($L_o = 2\pi/k_o$).

[1] M. Lazzari, M. A. Lopez-Quintela, *Adv. Mater.* **2003**, *15*, 1583.

[2] R. A. Segalman, *Mater. Sci. Eng. R* **2005**, *48*, 191.

[3] C. T. Black, *Appl. Phys. Lett.* **2005**, *87*, 163 116.

[4] C. T. Black, K. W. Guarini, K. R. Milkove, S. M. Baker, T. P. Russell, M. T. Tuominen, *Appl. Phys. Lett.* **2001**, *79*, 409.

[5] R. R. Li, P. D. Dapkus, M. E. Thompson, W. G. Jeong, C. Harrison, P. M. Chaikin, R. A. Register, D. H. Adamson, *Appl. Phys. Lett.* **2000**, *76*, 1689.

[6] J. Y. Cheng, C. A. Ross, V. Z. H. Chan, E. L. Thomas, R. G. H. Lammertink, G. J. Vancso, *Adv. Mater.* **2001**, *13*, 1174.

[7] K. Guarini, C. T. Black, Y. Zhang, I. V. Babich, E. M. Sikorski, L. M. Gignac, in *Proc. 49th IEEE Int Electron Devices Meeting*, IEEE, New York **2003**, p. 22.2.1.

[8] K. Naito, H. Hieda, M. Sakurai, Y. Kamata, K. Asakawa, *IEEE Trans. Magn.* **2002**, *38*, 1949.

[9] C. Harrison, M. Park, P. M. Chaikin, R. A. Register, D. H. Adamson, *J. Vac. Sci. Technol. B* **1998**, *16*, 544.

[10] T. Thurn-Albrecht, R. Steiner, J. DeRouchey, C. M. Stafford, E. Huang, M. Bal, M. Tuominen, C. J. Hawker, T. Russell, *Adv. Mater.* **2000**, *12*, 787.

[11] C. Harrison, Z. Cheng, S. Sethuraman, D. A. Huse, P. M. Chaikin, D. A. Vega, J. M. Sebastian, R. A. Register, D. H. Adamson, *Phys. Rev. E: Stat., Nonlinear, Soft Matter Phys.* **2002**, *66*, 011 706.

[12] C. Harrison, D. E. Angelescu, M. Trawick, Z. D. Cheng, D. A. Huse, P. M. Chaikin, D. A. Vega, J. M. Sebastian, R. A. Register, D. H. Adamson, *Europhys. Lett.* **2004**, *67*, 800.

[13] R. A. Segalman, A. Hexemer, E. J. Kramer, *Phys. Rev. Lett.* **2003**, *91*, 196 101.

[14] H. Furukawa, *Adv. Phys.* **1985**, *34*, 703.

[15] J. D. Gunton, M. San Miguel, P. S. Sahni, in *Phase Transitions and Critical Phenomena*, Vol. 8 (Eds: C. Domb, J. L. Lebowitz), Academic, New York **1983**.

[16] D. Boyer, J. Vinals, *Phys. Rev. E: Stat., Nonlinear, Soft Matter Phys.* **2001**, *64*, 050 101.

[17] D. Boyer, J. Vinals, *Phys. Rev. E: Stat., Nonlinear, Soft Matter Phys.* **2002**, *65*.

[18] H. Qian, G. F. Mazenko, *Phys. Rev. E: Stat., Nonlinear, Soft Matter Phys.* **2003**, *67*, 036 102.

[19] F. Liu, N. Goldenfeld, *Phys. Rev. A: At., Mol., Opt. Phys.* **1989**, *39*, 4805.

[20] Y. Shiwa, *Phys. Rev. E: Stat Phys., Plasmas, Fluids, Relat. Interdiscip. Top.* **2000**, *61*, 2924.

[21] A. G. Xu, G. Gonnella, A. Lamura, G. Amati, F. Massaioli, *Europhys. Lett.* **2005**, *71*, 651.

[22] Y. Yokojima, Y. Shiwa, *Phys. Rev. E: Stat., Nonlinear, Soft Matter Phys.* **2002**, *65*.

[23] A. Hoffmann, J.-U. Sommer, A. Blumen, *J. Chem. Phys.* **1997**, *107*, 7559.

[24] C. Harrison, D. H. Adamson, Z. Cheng, J. M. Sebastian, S. Sethuraman, D. A. Huse, R. A. Register, P. M. Chaikin, *Science* **2000**, *290*, 1558.

[25] B. A. Garetz, N. P. Balsara, H. J. Dai, Z. Wang, M. C. Newstein, B. Majumdar, *Macromolecules* **1996**, *29*, 4675.

[26] E. Huang, P. Mansky, T. P. Russell, C. Harrison, P. M. Chaikin, R. A. Register, C. J. Hawker, J. Mays, *Macromolecules* **2000**, *33*, 80.

[27] P. Mansky, Y. Liu, E. Huang, T. P. Russell, C. Hawker, *Science* **1997**, *275*, 1458.

[28] S. H. Anastasiadis, T. P. Russell, S. K. Satija, C. F. Majkrzak, *Phys. Rev. Lett.* **1989**, *62*, 1852.

[29] C. T. Black, K. W. Guarini, *J. Polym. Sci. Part A* **2004**, *42*, 1970.

[30] K. A. Cavicchi, T. P. Lodge, *Macromolecules* **2004**, *37*, 6004.

[31] M. C. Dalvi, C. E. Eastman, T. P. Lodge, *Phys. Rev. Lett.* **1993**, *71*, 2591.

[32] D. Ehlich, M. Takenaka, S. Okamoto, T. Hashimoto, *Macromolecules* **1993**, *26*, 189.

[33] M. W. Hamersky, M. A. Hillmyer, M. Tirrell, F. S. Bates, T. P. Lodge, E. D. von Meerwall, *Macromolecules* **1998**, *31*, 5363.

[34] T. P. Lodge, M. C. Dalvi, *Phys. Rev. Lett.* **1995**, *75*, 657.

[35] K. R. Shull, E. J. Kramer, *Macromolecules* **1991**, *24*, 1383.

[36] M. Doi, S. F. Edwards, *The Theory of Polymer Dynamics*, Oxford University Press, New York **1986**.

[37] H. Yokoyama, E. J. Kramer, *Macromolecules* **1998**, *31*, 7871.

[38] J. D. Ferry, *Viscoelastic Properties of Polymers*, Wiley, New York **1980**.

[39] M. Kleman, O. D. Lavrentovich, *Soft Matter Physics. An Introduction*, Springer, New York **2003**.

[40] P.-G. de Gennes, J. Prost, *The Physics of Liquid Crystals*, Oxford University Press, New York **1993**.

[41] J. Hahm, S. J. Sibener, *J. Chem. Phys.* **2001**, *114*, 4730.

[42] M. R. Hammond, E. J. Kramer, *Macromolecules* **2006**, *39*, 1538.

[43] L. Rockford, Y. Liu, P. Mansky, T. P. Russell, M. Yoon, S. G. J. Mochrie, *Phys. Rev. Lett.* **1999**, *82*, 2602.

[44] S. O. Kim, H. H. Solak, M. P. Stoykovich, N. J. Ferrier, J. J. de Pablo, P. F. Nealey, *Nature* **2003**, *424*, 411.

[45] M. P. Stoykovich, M. Muller, S. O. Kim, H. H. Solak, E. W. Edwards, J. J. de Pablo, P. F. Nealey, *Science* **2005**, *308*, 1442.

[46] S. B. Darling, N. A. Yufa, A. L. Cisse, S. D. Bader, S. J. Sibener, *Adv. Mater.* **2005**, *17*, 2446.

[47] C. T. Black, O. Bezencenet, *IEEE Trans. Nanotechnol.* **2004**, *3*, 412.

[48] D. Sundrani, S. B. Darling, S. J. Sibener, *Nano Lett.* **2004**, *4*, 273.

[49] D. Sundrani, S. B. Darling, S. J. Sibener, *Langmuir* **2004**, *20*, 5091.

[50] C. Harrison, P. M. Chaikin, D. A. Huse, R. A. Register, D. H. Adamson, A. Daniel, E. Huang, P. Mansky, T. P. Russell, C. J. Hawker, D. A. Egolf, I. V. Melnikov, E. Bodenschatz, *Macromolecules* **2000**, *33*, 857.